Article ID: 1006-8775(2023) 01-0026-13

Organizational Modes and Environmental Conditions of the Severe Convective Weathers Produced by the Mesoscale Convective Systems in South China

ZHANG Yuan-chun (张元春)[1], LU Rong (鲁 蓉)[2], SUN Jian-hua (孙建华)[1, 3], YANG Xin-lin (杨新林)[4]

(1. Key Laboratory of Cloud-Precipitation Physics and Severe Storms, Institute of Atmospheric Physics, Chinese Academy of Sciences, Beijing 100029 China; 2. Nanjing Meteorological Bureau, Nanjing 210009 China; 3. University of Chinese Academy of Sciences, Beijing 100049 China; 4. College of Aviation Meteorology, Civil Aviation Flight University of China, Guanghan, Sichuan 618399 China)

Abstract: Composite radar reflectivity data during April - September 2011−2015 are used to investigate and classify storms in south China (18−27°N; 105−120°E). The storms appear most frequently in May. They are either linear; cellular or nonlinear systems, taking up 29.45%, 24.51% and 46.04%, respectively, in terms of morphology. Linear systems are subdivided into six morphologies: trailing stratiform precipitation (TS), bow echoes (BE), leading stratiform precipitation (LS), embedded line (EL), no stratiform precipitation (NS) and parallel stratiform precipitation (PS). The TS and NS modes have the highest frequencies but there are only small samples of LS (0.61%) and PS (0.79%) modes. Severe convective wind (≥17m s^{-1} at surface level) accounts for the highest percentage (35%) of severe convective weather events produced by cellular systems including individual cells (IC) and clusters of cells (CC). Short-duration heavy rainfall (≥50 mm h^{-1}) and severe convective wind are the most common severe weather associated with TS and BE modes. Comparison of environmental physical parameters shows that cellular convection systems tend to occur in the environment with favorable thermal condition, substantial unstable energy and low precipitable water from the surface to 300 hPa (PWAT). However, the environmental conditions favoring the initiation of linear systems feature strong vertical wind shear, high PWAT, and intense convective inhibition. The environmental parameters favoring the initiation of nonlinear systems are between those of the other two types of morphology.

Key words: storms; composite reflectivity; morphology; severe convective weather; environmental physical parameter

CLC number: P44 **Document code:** A

Citation: ZHANG Yuan-chun, LU Rong, SUN Jian-hua, et al. Organizational Modes and Environmental Conditions of the Severe Convective Weathers Produced by the Mesoscale Convective Systems in South China [J]. Journal of Tropical Meteorology, 2023, 29(1): 26-38, https://doi.org/10.46267/j.1006-8775.2023.003

1 INTRODUCTION

Severe convective weather (SCW), such as short-duration heavy rainfall (SDHR), severe convective winds, and hail, appears frequently in China. Many previous studies focused on the occurrence and development of SCW (Maddox [1]; Tao [2]; Houze Jr [3]; Zhang et al. [4]; Xie et al. [5]; Yu et al. [6]; Zheng et al. [7]). Additionally, it is suggested that SCWs are mostly produced by mesoscale convective systems (MCSs, Maddox [1]; Tollerud and Collander [8]; Doswell [9]; Schumacher and Johnson [10]; Shibagaki et al. [11]). With the advances in satellite remote sensing and radar detection, high spatial and temporal resolution datasets, particularly the stationary satellite observation data with longer time series, higher resolution and better quality control, have been applied to explore the spatial and temporal distribution of MCSs all over the world. (Maddox [1]; Zheng et al. [7]; Augustine and Howard [12]; Laing and Fritsch [13]; Anderson and Arritt [14]; Jirak et al. [15]; Goyens et al. [16]; Zhuo et al. [17]). Maddox [1] defined mesoscale convective complexes (MCCs) using infrared satellite data, with the criteria of temperature of black body (TBB) ⩽ −32 ℃ and cloud area ⩾ 10^5 km^2, and TBB⩽ −52 ℃ and cloud area ⩾ 5×10^4 km^2. Based on the definition of Maddox [1], Jirak et al. [15] removed the ⩽ −32 ℃ size requirement of the satellite classification scheme in Maddox [1] and further divided the MCSs into four morphologies. Although the infrared satellite data were useful for MCSs' identification and tracking, radar imagery can show the development and three-dimensional structure of MCSs in detail, especially the spatial distributions of convective and stratiform development (Zheng et al. [7]; Schumacher and Johnson [10]; Jirak et al. [15]; Parker and Johnson [18]; Meng et al. [19]; Li et al. [20], Chen et al. [21]).

Numerous studies have used radar data to classify the morphologies of MCSs (e.g., Zheng et al. [7]; Jirak et

Received 2022-09-14; **Revised** 2022-11-15; **Accepted** 2023-02-15

Funding: National Key Research and Development Program of China (2019YFC1510400); National Natural Science Foundation of China (41975056, 41675045)

Biography: ZHANG Yuan-chun, Associate Research Fellow, primarily undertaking research on mesoscale meteorology.

Corresponding author: ZHANG Yuan-chun, e-mail: zhyc@mail.iap.ac.cn

al.[15]; Parker and Johnson[18]; Bluestein and Jain[22]; Blanchard[23]; Loehrer and Johnson[24]; Wang et al.[25]; Yang and Sun[26]). In some earlier studies, severe and non-severe squall lines were documented into four distinct formation modes: broken line, back building, broken area and embedded area (Bluestein and Jain[22]). Parker and Johnson[18] proposed three morphologies for linear convective systems: trailing stratiform precipitation (TS), leading stratiform precipitation (LS) and parallel stratiform precipitation (PS). Based on the above three morphologies of linear convective systems, Gallus Jr et al.[27] classified MCSs into nine morphologies according to the dominant morphology in the radar data, adding individual cells (IC), clusters of cells (CC), broken lines (BL), bow echoes (BE), no stratiform precipitation (NS), and nonlinear systems. It was found that the nine dominant morphologies covered almost all common mesoscale convective storms. Jirak et al.[15] further studied the different patterns of MCSs and classified MCSs into 17 morphologies during the active convective season of the central United States. Some studies examined the organizational modes of MCSs over central east China (Zheng et al.[7]; Wang et al.[25]). Zheng et al.[7] classified the MCSs over central east China into NL and six linear organizational modes: NS, TS, LS, PS, BE, and embedded lines (EL). A statistical analysis of MCSs over Yangtze River Basin found eight morphologies of linear modes: TS, LS, training line/adjoining stratiform, back-building/quasi-stationary MCSs (BB), PS, BL, EL and long line. Yang and Sun[26] collected the severe-wind-producing convective system events over north China and concluded six organizational modes that consist of CC (35.4%), squall lines (18.4%), nonlinear-shaped systems (17.8%), BL (11.6%), IC (1.2%) and BE (0.5%). Recent studies also analyzed the features of MCSs associated with warm-sector heavy rainfall and quasi-linear MCSs in south China. Li et al.[20] examined the organizational modes of mesoscale convective systems (MCSs) associated with warm-sector heavy rainfall events in south China and found that these MCSs can be classified into NL (40%) and eight linear modes (60%): TS, NS, LS, PS, EL, BE, training line/adjoining stratiform, and multiple rain bands (MRB). Chen et al.[21] analyzed the general features and circulation patterns of 98 quasi-linear MCSs over south China, which include TS (39.8%), NS (22.4%), EL(11.2%), PS(10.2%) and multiple convective lines with stratiform precipitation (MLS, 16.3%).

It was shown that different morphologies of MCSs corresponded to different SCWs, such as heavy rainfall, hail, high wind and tornadoes (Zheng et al.[7]; Parker and Johnson[18]; Bluestein and Jain[22]; Yang and Sun[26]; Gallus Jr et al.[27]; Parker[28]; Duda and Gallus Jr[29]; Lombardo and Colle[30];). Fujita[31] demonstrated that bow echoes tended to produce more high wind events. Tornadoes were often observed in bow echoes (Trapp et al.[32]) and supercells (Moller et al.[33]). Pettet and Johnson[34] showed that LS and PS squall lines produced more flooding events. It was also found that training line/adjoining stratiform and BB were the two most frequent modes in the 116 extreme rainfall events from 1999 to 2001 in the east of the Rocky Mountains in the United States (Schumacher and Johnson[10]). Duda and Gallus Jr[29] analyzed severe weather reports as a function of convective mode and found substantial differences between the morphologies of severe weather reports and different storm morphologies. Over central east China, BE systems generate the most severe weather on average, while most TS systems are attendant with SDRH and high winds. EL and PS systems are most frequently associated with extreme SDHR (Zheng et al.[7]).

Additionally, the classification of MCSs may be associated with various dynamical and thermal conditions (Zheng et al.[7]; Parker and Johnson[18]; Bluestein and Jain[22]; Yang and Sun[26]; Gallus Jr et al.[27]; Parker[28]; Duda and Gallus Jr[29]; Lombardo and Colle[30]). It has been demonstrated that vertical wind shear is an important factor to distinguish different morphologies of convection systems (Parker and Johnson[18]). It was shown that the type of BE over central east China generally occurs under strong low-level vertical shears. The LS and PS tended to produce flooding events. The physical parameters derived from the environmental soundings of MCSs were compared over different regions between east China and the central United States (Zheng et al.[7]). Precipitable water (PWAT) was another key factor to affect the convection-producing SCWs. It was proposed that PWAT of TS mode is higher than that of LS and PS over the central United States (Parker and Johnson[18]). The high PWAT in moist MCSs over central east China shows great similarity to the results of pre-tropical cyclone (TC) squall lines that occurred over south China (Meng et al.[19]; Meng and Zhang[35]). Zheng et al.[7] also found that severe convective winds and hail events were mainly observed in dry environments (PWAT $\leqslant$ 50 mm) and SDHR occurred more frequently in moist environments (PWAT $\geqslant$ 50 mm). Different PWAT values correspond to different convection modes, such as 28 mm for convection lines (Bluestein and Jain[22]), 26.9 mm for severe convective windstorms, 33.5 mm for TS mode, 32.7 mm for LS systems, and 24.3 mm for PS type (Parker and Johnson[18]). In addition, thermal environmental conditions were also essential for convection initiation, consisting of surfaced-based convective available potential energy (SBCAPE), lifted index (LI), and lifting condensation level (LCL).

The above recent studies mainly explored the classification features, SCWs and environmental conditions of MCSs in both the east and north China, however, few studies focused on these characteristics of MCSs in south China. It is well known that different

synoptic background systems can influence the differences of the organization modes, corresponding SCWs and environmental conditions of MCSs over different regions. The main synoptic systems over south China include a southwesterly low-level jet (LLJ) originated over the tropical oceans, a low-level vortex developing in southwest China and a subtropical high over the northwestern Pacific (WPSH) (Tao and Ding [36]; Ninomiya and Akiyama [37]), which are different with those in both the east and north China. It is essential to explore the general features of MCSs in south China. The goal of this study is to investigate morphologies of MCSs, their corresponding SCWs and the environmental conditions in south China.

Section 2 introduces data and methodology. Morphologies of radar echoes in south China are shown in section 3. Two SCW events corresponding to each morphology mode are compared in section 4. Section 5 analyzes the environmental conditions before convection initiation of different morphologies. Finally, the conclusion is given in section 6.

2 DATA AND METHODOLOGY

2.1 *Composite radar reflectivity and severe weather reports*

Composite Doppler radar reflectivity from April to September of 2011−2015 are used to derive and classify MCSs over south China (18−27°N, 105−120°E, Fig. 1). These composite radar reflectivity data with 10-min temporal and 1 km × 1 km spatial resolutions were provided by the National Meteorological Center (NMC) of the China Meteorological Administration (CMA). Meanwhile, hourly automatic weather station data and 3-hourly severe weather reports are used to analyze severe weather events. According to the definition of NMC, SCW refers to SDHR with hourly precipitation amount ⩾ 20 mm h^{-1}, and severe convective winds with speeds higher than or equal to Beaufort scale 8 (or 17.2 m s^{-1}), hail and any tornado, but tornadoes were not considered in this study. The SDHR events are obtained from the automatic weather station data, and severe convective winds and hail events are obtained from severe weather reports. Because of the localization of severe convective winds and hail, these events cannot be fully recorded in automatic weather station data, which report the general occurrence and geographic distribution features of the two SCW events.

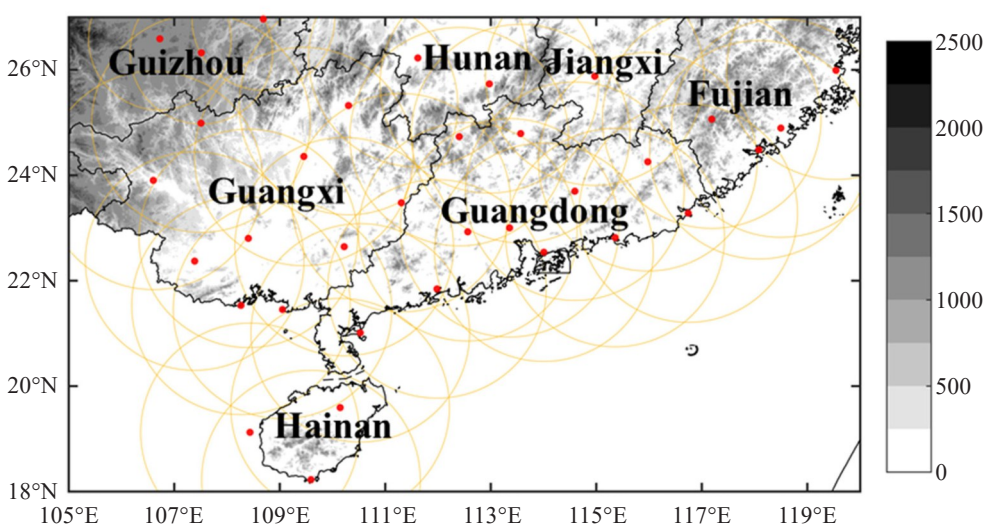

Figure 1. Regional and topographic (shading, units: m) distributions of the study areas. The red dots represent the radar stations and the yellow circles with a radius of 200 km are centered at the radar stations representing their scanning ranges.

2.2 *Classification of radar echo morphologies*

Herein the lifetime of a storm was subjectively determined by the start (end) time of the first (last) radar image where the 30-dBZ contiguous echo coverage exceeded a 30 km ×30 km area with a maximum exceeding 45 dBZ for at least 1 h (Zheng et al. [7]). Except for the missing and discontinuous radar mosaic, 1640 reflectivity samples are collected, comprising 208, 267, 251, 459 and 455 samples for 2011, 2012, 2013, 2014 and 2015, respectively (Table 1). Convective and stratiform echoes were defined as those of greater than 40 and 20−40 dBZ, respectively (Parker and Johnson [18]; Geerts [38]). As the pattern of radar echoes varied over the lifetime of a convective system, one individual storm could be classified into different morphologies at its different evolution stages. The classification scheme used in the present study was basically the same as that in G08 except the embedded lines (ELs) as they are a common morphology in China (Zheng et al. [7]; Li et al. [20]; Chen et al. [21]; Wang et al. [25]). The storm morphologies were classified into three types, namely, cellular, linear, and nonlinear systems. The cellular systems were subdivided into individual cells (ICs) and clusters of cells (CCs). ICs were storms without weaker

radar echoes (10 dBZ < radar echoes < 40 dBZ) connecting the cells. CCs were storm cells connected by weaker radar echoes. Linear systems were those in which the convective echoes were connected and organized in a linear shape of at least 100 km in length and a length-to-width ratio of at least 3: 1, with these features lasting for at least 1 h. The criteria for linear systems were essentially the same as those in previous studies (Zheng et al. [7]; Chen et al. [21]; Gallus Jr et al. [27]; Yang et al. [39]). The linear systems included six subtypes: trailing stratiform (TSs), leading stratiform (LSs), parallel stratiform (PSs), no stratiform (NSs), bow echoes (BEs) and ELs, which is different from the five organization modes of quasi-linear MCSs , including TSs, NSs, PSs, ELs and MLSs (Chen et al. [21]). A schematic diagram illustrating the classified storm morphologies is given in Fig. 2.

Table 1. Sample distributions of nine storm morphologies.

Category	2011	2012	2013	2014	2015	Total
IC	17	8	10	9	24	68
CC	60	50	47	136	122	415
TS	8	48	28	34	46	164
PS	2	1	4	5	1	13
LS	0	6	0	2	2	10
BE	1	6	4	6	5	22
EL	12	24	16	18	14	84
NS	9	21	19	32	28	109
NL	99	103	123	217	213	755
Total	208	267	251	459	455	1640

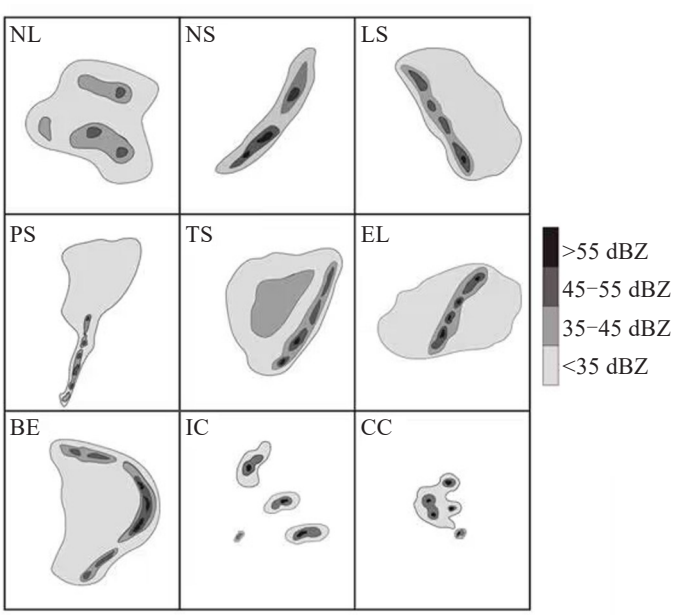

Figure 2. Schematic illustrations of radar echo morphologies: individual cells (ICs) and clusters of cells (CCs), nonlinear systems (NLs), convective lines with trailing stratiform (TSs), convective lines with leading stratiform (LSs), convective lines with parallel stratiform (PSs), convective lines with no stratiform (NSs), bow echoes (BEs) and embedded lines (Els).

2.3 *Creating proximity soundings*

To explore the environmental conditions associated with various storm morphologies, the environmental physical parameterizations are calculated three hours prior to convection initiation. Because the temporal and spatial resolutions of sounding observation are coarse and most SCWs occur in the afternoon and at night, the sounding observations are too coarse to capture the

environment of a SCW event. The thermodynamic soundings are reconstructed using global final-analysis data from National Centers for Environmental Prediction (NCEP FNL, 6-h temporal and 1 °×1 ° spatial resolutions) to create proximity soundings (Lee [40]; Brooks et al. [41]). Considering the large errors between the model near surface level and observations, the surface observation data from automatic weather stations is applied to represent the signals in the lower atmosphere of the reanalysis data (Johnson and Bresch [42]; Pan et al. [43]). The time, at which the sounding is reconstructed, is within three hours prior to the initiation of convective systems. For example: the reanalyzed vertical data (FNL) at 08 BST (Beijing Standard Time, BST=UTC+8 h) is revised using the surface observations at 08 and 11 BST; the vertical data at 14 BST are modified using the surface observation at 14 and 17 BST. Additionally, the revised sounding spot is within 100 km of the station or grid point that is the nearest to the convective initiation location.

2.4 *Environmental physical parameters*

The fundamental conditions for the initiation and development of convection include moisture, instability and lifting. Additionally, the vertical wind shear is also important for the organized convection (Parker and Johnson [18]). Nine physical parameters, including dynamic, thermal and thermo-dynamic conditions, are chosen to indicate the environmental conditions three hours prior to storms: surface-based convective available potential energy (SBCAPE), most unstable convective available potential energy (MUCAPE), downdraft convective available potential energy (DCAPE), surface-based convective inhibition (SBCIN), most unstable convective inhibition (MUCIN), lifting index (LI), precipitable water from surface to 300 hPa (PWAT), 0−3 km vertical wind shear (VWS_3 km), 0-6 km vertical wind shear (VWS_6 km).

3 STORM MORPHOLOGIES OF RADAR ECHOES

3.1 *Storm organizational modes*

According to the definition in Section 2.2, 1640 radar echo samples from April to September of 2011−2015 are selected and classified into three main morphologies: linear systems (402 cases), cellular systems (483 cases) and nonlinear systems (755 samples). The sample numbers of the storm organizational modes are listed in Table 1. Among all the derived samples, NLs (755) are the most common, accounting for 46.03%. This percentage is similar to those (44.7%) over central east China (Zheng et al. [7]). The cellular systems combined with ICs and CCs are 483, constituting 29.45% of all the cases. All the remaining samples (402 cases, 24.51%) are linear systems. As can be seen from the pie chart in Fig. 3, the most prevalent linear systems are TSs, NSs and ELs, with percentages of 10.00%, 6.65% and 5.12%, respectively. Similar results are also found in Chen et al. [21], which focuses on the quasi-linear MCSs. The percentage of BEs is 1.34% and the smallest samples are PSs (0.79%) and LSs (0.61%). The small contribution of LSs to the total number is similar to that in central east China (Zheng et al. [7]) and the central United States (Gallus Jr et al. [27]; Duda and Gallus Jr [29]).

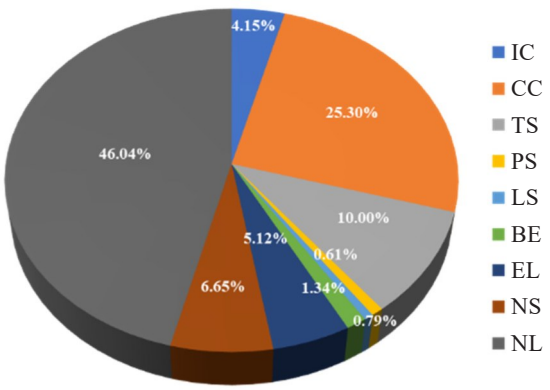

Figure 3. Percentages of various storm morphologies.

3.2 *Monthly variation and duration*

In General, storm samples over south China are relatively small in April and September, while the frequency of storms is the greatest in May, with the second highest number in June (Fig. 4). The highest frequency of storms in May could be related to the pre-summer rainy season in south China (Luo [44]). For individual morphologies, the frequency of CCs is much higher than that of ICs. The two highest frequency of CC is in July and August. The two highest frequencies of TSs are in May and June, with the frequency in September being the smallest. Both LS and EL modes have their highest frequency in May, with a second peak in April. The highest frequency of BE mode is also in May, while the numbers in April and June are nearly the same. By contrast, NS mode occurs mostly in August, with June in the second place. The frequency of PS mode is relatively small throughout the study period, but there are peaks in May and August. For NL mode, the

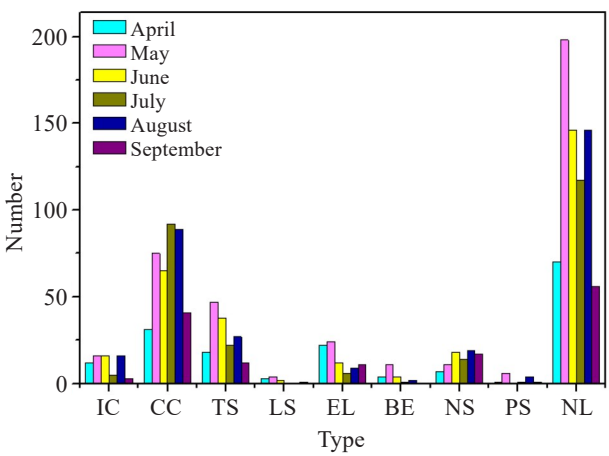

Figure 4. Monthly distributions of various storm morphologies.

highest frequency is in May, with smaller peaks in June and August. Among the nine morphologies, the highest frequency of seven modes is in May, indicating that the convective activity in the pre-summer rainy season is the strongest.

As the frequency of each type of linear storms is small, we just discuss the duration of cellular, linear and nonlinear systems. The durations of the storms concentrate on 1−3 hours and 3−6 hours, however, the lifetimes of the different storm morphologies vary considerably (Fig. 5). The durations of linear systems are concentrated in the range of 1−3 hours, whereas those of the NL mode lie mainly between 3 and 6 hours. The case numbers of cell morphology maintaining for 1−3 hours are similar to the number of this type of convection systems that last for 3−6 hours. Compared with cellular and linear systems, there are much more events of NL mode which have lifetimes longer than 6 hours.

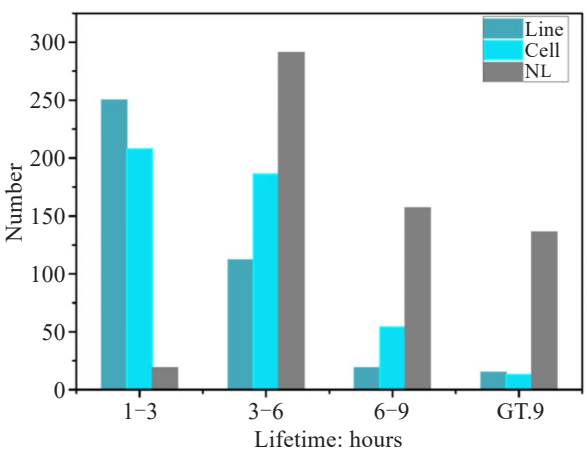

Figure 5. Life cycles of three storm morphologies.

3.3 *Geographical distribution of convection initiation*

To explore the environmental and circulation features of different storm morphologies, it is necessary to analyze the locations at which each category is initiated. The initiation time is defined as the time at which the maximum composite reflectivity reaches 45 dBZ and the coverage of 30 dBZ is greater than 30 km × 30 km. The initiation location is taken as the centroid point of the strongest echo or, if the strongest echoes are scattered, as the geometric center of these echoes.

In south China, IC and CC samples are mainly concentrated over coastal regions of Guangdong and Guangxi (Fig. 6). It has been found that coastal terrain and the land-sea contrast are crucial for convection initiation (Luo [44]; Wu and Luo [45]; Bai et al. [46]). The NSs occur more frequently over the coastal regions of Guangdong and the southern area of Guangxi, which is next to Beibu Gulf. Wang et al. [25] found that a mesoscale boundary between precipitation-induced cold outflows and warm air from the South China Sea and Beibu Gulf was important for the triggering of fresh convection. The TSs are generated over wider areas, with its highest frequency of occurrence being over the junction regions between Guangdong and Guangxi. The initiation locations of BEs and ELs are concentrated over the western part of Guangxi (the eastern edge of Yungui Plateau) and the coastal regions of Guangdong and Hainan, although the ELs have another high frequency in Beibu Gulf. The PSs and LSs are mainly generated in Guangdong and the coastal region (their frequency distributions are not shown in Fig. 6 because of the few samples). The NLs, which contribute the largest percentage of all the radar echoes, appear more over the coastal regions of Guangdong, the southern boundary regions of Guangdong and Guangxi, and the middle part of Guangxi. The general geographic distributions of all the categories show that storms are mainly initiated over the middle and northern regions of Guangdong (the windward slopes of the mountainous areas), the southern boundary regions of Guangdong and Guangxi, and the southern part of Guangxi (with a trumpet-shaped topography). These distributions indicate that the topography has a great influence on the convective initiation. Some case studies found that both coastal convergence and topographic lifting can influence convection initiation over the southern coast of China (Luo [44]; Chen et al. [47]; Du and Chen [48], Du et al. [49]).

In summary, the geographical distribution of each category has the following features: the linear systems are initiated mainly over mountainous and coastal regions, the ICs tend to occur over the plains, and the CCs and NLs are more evenly distributed.

4 SEVERE CONVECTIVE WEATHER ASSOCIATED WITH STORM MORPHOLOGIES

The combination of storm morphologies and SCW events (SDHR, severe convective winds and hail) is further investigated in this section. SDHR is an SCW type with the highest frequency and widely spread in China. Severe convective winds mostly occur in north China and Guangdong (Yang et al. [50]) whereas hails occur more frequently in mountains and plateaus, with relatively low frequency in south China (Li et al. [51]). According to the definition of SCW by the NMC, the minimum criterion for SCW is that the rainfall intensity of SDHR should be more than 20 mm h^{-1}, but considering the local hourly precipitation intensities in south China, this is amended to 50 mm h^{-1} (Chen et al. [52]). When the instantaneous maximum wind reaches 17 m s^{-1}, an SCW event is defined as severe convective wind. All the hail reports are included because of low frequency of hail in south China. The SCWs corresponding to all the radar echo samples (1640) are derived here. The main SCWs differ among the various storm morphologies (Fig. 7a). Severe convective winds ("wind" in the legend of Fig. 7) contribute the highest percentage (>35%) of the weather phenomena induced

by the ICs and CCs, and the severe convective winds percentage of IC reaches up to 50%. SDHR ("rain" in the legend of Fig. 7) and severe convective winds are the most common weather phenomenon associated with the TSs and BEs: the percentage of rain being higher than 45% and severe convective winds accounting for more than 25%. The main samples of LSs and Els produce SDHR (with respective percentages being ~70% and 45%), while the severe convective wind percentages are about 10%. Similar to the SCW associated with the PS mode described in Zheng et al.[7], there are no hail events associated with the PS mode in central east China, which contrasts with the significant hail reports in the United States. It is also clearly shown that hail events only appear in IC, CC and NS systems, but NS and BE systems are the leading producers of hail events in central east China (Zheng et al.[7]). SDHRs and severe convective winds are associated with just a small percentage of this type of radar echo. SDHR accompanying with severe convective winds could occur in all the morphologies (Fig. 7b). ICs and CCs can produce SDHR and hail events simultaneously. For CCs, TSs and NSs, hail could appear with SDHR and severe convective winds at the same time.

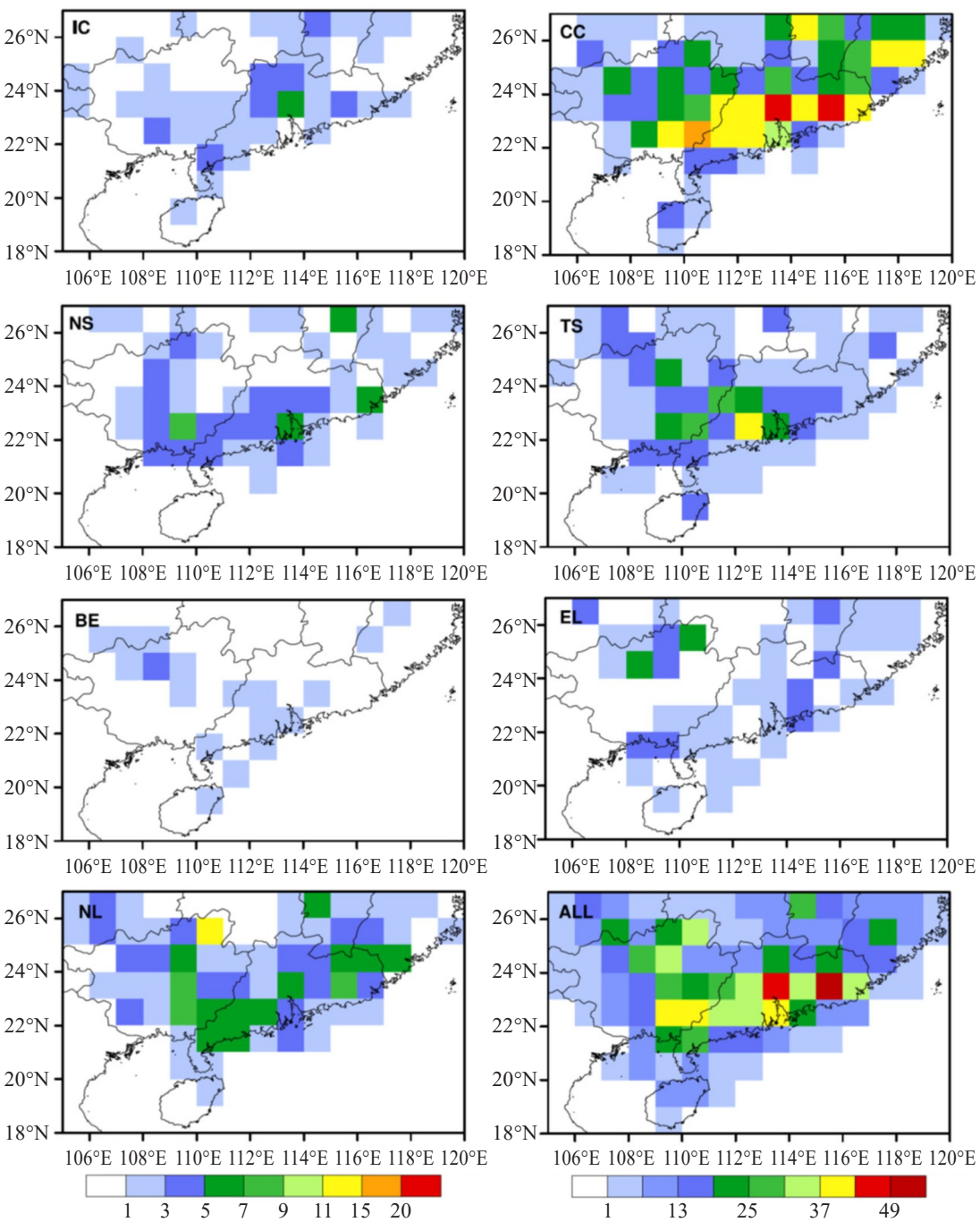

Figure 6. Frequency distributions (in number of occurrences) of initiation locations for various storm morphologies: IC, CC, NS, TS, BE, EL, NL and all morphologies in sequence.

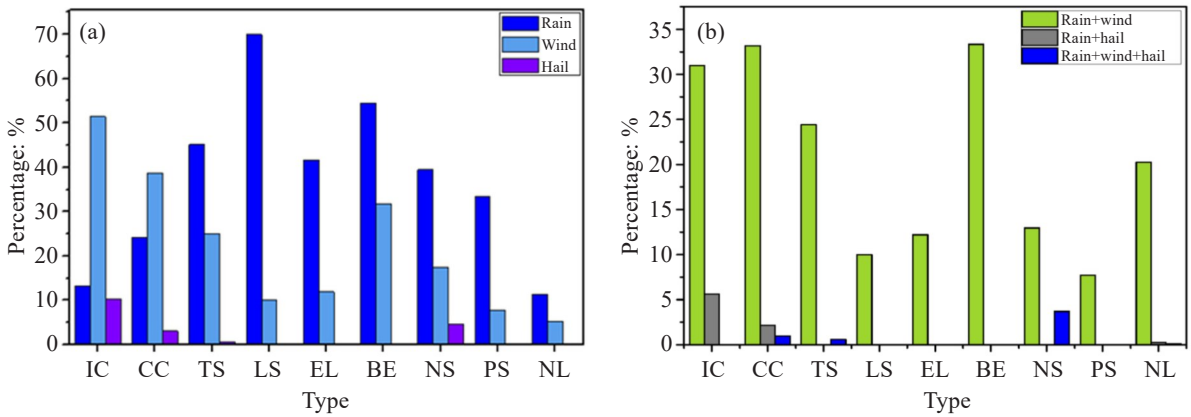

Figure 7. Percentages of different weather phenomena associated with various storm morphologies (the precipitation criterion is a minimum of 50 mm h^{-1}). (a) Percentages of each weather phenomenon; (b) percentages of various weather phenomena occurring simultaneously.

On the other hand, Fig. 8 illustrates the percentage distributions of storm morphologies for the three main SCW events. For severe convective winds, the CC mode accounts for the highest percentage, with the NL mode in the second place (Fig. 8a). This feature is partly similar to the results in north China, while the percentage of CCs is the highest associated with severe convective winds. In central east China, however, BE systems had the highest probability of severe convective winds, especially significant severe convective winds (≥ 24 m s^{-1}) (Zheng et al. [7]). It was also demonstrated that bow echoes tended to produce more severe convective winds reports in the United States (Gallus Jr et al. [27]). However, since the number of samples of the NLs is much greater than those of other morphologies, the percentage of severe convective winds cases is not high among NL mode samples. The percentages for the ICs and TSs are near 10%. SDHR is mostly associated with the NLs, while the CCs, and TSs each account for more than 10% (Fig. 8b). The proportions of other storm morphologies are below 10%. The highest percentage of hail is associated with the CCs (>40%), while the ICs, NSs and NLs each account for more than 10% (Fig. 8c).

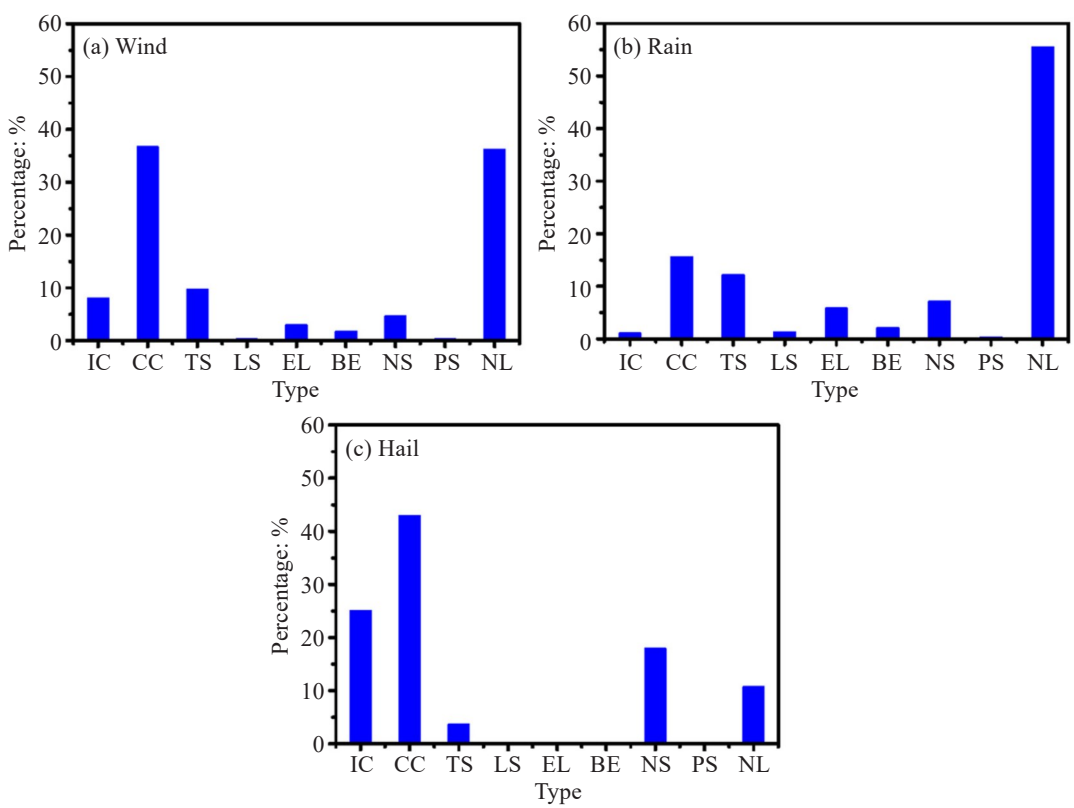

Figure 8. Proportions of various storm morphologies producing SCW events: (a) severe convective winds; (b) SDHR; (c) hail.

5 ENVIRONMENTAL CONDITIONS ASSOCIATED WITH INITIATION OF STORMS

The physical parameters listed in section 2.4 are related to moisture conditions (PWAT), thermal (SBCAPE, MUCAPE, DCAPE, SBCIN, MUCIN, LI, etc.), and dynamic (VWS_3km, VWS_6km) conditions.

Table 2 lists the average physical parameters of all linear systems. A comparison among these parameters shows that the BE mode has the highest values of SBCIN and MUCIN (thermal conditions) and of VWS_6km (dynamical conditions), indicating that when more unstable energy is accumulated before the initiation of convection, accompanied by simultaneous intense vertical wind shear, the convection can develop into strong convective systems after initiation. The TSs account for the highest percentage of general linear modes. From a comparison of its parameters with those of other morphologies, it is found that the absolute LI of the TS mode is the second greatest, but the vertical wind shear (VWS_3km and VWS_6km) is not very intense. For this mode, SBCAPE, DCAPE and the moisture conditions (PWAT) all lie in the middle range. After the TS mode, the NS mode has the greatest number of linear samples. This mode is associated with a high frequency of occurrence of severe convective winds and hail, characterized by strong updraft and downdraft (as indicated by the large SBCAPE and DCAPE and small SBCIN) and weak vertical wind shear (as indicated by the small VWS_3km and VWS_6km). These environmental conditions indicate that the NSs occur in environments with high convective energy and weak vertical wind shear, causing weak tilting of vertical motion, which can explain the non-stratiform region. Among the other morphologies, the ELs have the smallest SBCAPE and the second smallest DCAPE, but relatively large SBCIN and MUCIN, which means that this convection system needs strong triggering conditions for its development. The high PWAT of the ELs means that this system occurs when moisture conditions are favorable. The environmental wind vertical shear of the ELs has a medium value, which is greater than those of the TS and NS modes but smaller than that of BE mode.

Owing to the limited number of samples of the LSs in south China, it is possible that the features of the parameters may be affected to a certain extent. According to the results of the present calculation, the large SBCAPE, DCAPE and MUCAPE imply strong unstable energy, similarly to the NSs. Additionally, the small PWAT (3.7cm) reveals that the LSs mostly occur in relatively dry environments. The environmental wind shear (VWS_3km) of LSs are larger than that of other morphologies, which means that for the LSs to occur, high energy and strong vertical wind shear are necessary. This may be the reason of the low frequency of occurrence of LSs. The frequency of the PSs is even lower than that over central east China (Zheng et al.[7]). Compared with the environmental conditions of the LSs, the PSs have much lower SBCAPE, DCAPE and SBCIN but higher PWAT. Moreover, the vertical wind shear parameters are larger than those of other morphologies. These characteristics indicate that the derived PSs are mostly generated in wet environments featuring low convective energy but strong vertical wind shear.

Table 2. Average physical parameters of various linear morphologies.

Type	SBCAPE ($J\ kg^{-1}$)	MUCAPE ($J\ kg^{-1}$)	DCAPE ($J\ kg^{-1}$)	MUCIN ($J\ kg^{-1}$)	SBCIN ($J\ kg^{-1}$)	LI (K)	VWS_3km ($m\ s^{-1}$)	VWS_6km ($m\ s^{-1}$)	PWAT (mm)
BE	1382.1	1251.5	618.7	**69.8**	***75.4***	−3.0	17.1	***26.5***	4.3
TS	1843.0	1785.9	570.0	49.7	54.1	***−3.5***	**14.4**	**21.2**	4.1
NS	***2093.0***	1982.4	***663.7***	**41.9**	49.6	−3.5	**13.3**	**20.6**	3.8
EL	**1276.3**	1168.3	**549.4**	***61.9***	***69.3***	−2.3	16.8	24.8	4.3
LS	2114.4	2092.6	678.4	41.1	51.9	−3.8	17.2	24.7	**3.7**
PS	**1362.5**	1351.6	**364.6**	**18.0**	31.3	−2.3	***18.3***	***26.1***	***4.6***

In addition to the different SCW events associated with linear systems, cellular systems and nonlinear systems, respectively, there are also differences among their environmental parameters (Table 3). First of all, SBCAPE, MUCAPE, LI and other thermal and dynamic parameters of cellular systems are much larger than those of linear and nonlinear systems, suggesting that high values of thermal and unstable energy are more favorable for the initiation of cellular systems. Furthermore, the larger DCAPE of cellular systems indicates that stronger downdraft could produce severe convective winds and hail. Meanwhile, the smaller PWAT of cellular systems suggest that these occur in relatively dry environment with lower amounts of water vapor. Vertical wind shear (VWS_3km and VWS_6km) of the cellular systems is weaker than linear and nonlinear systems. It is possible that cellular systems (CCs and ICs) are more favorable to be initiated under

favorable thermal environmental conditions. The small SBCAPE of linear systems indicates that relatively low energy could also trigger this type of convection. The higher DCAPE of linear systems compared with nonlinear systems indicates a greater likelihood of severe convective winds for the former. On the other hand, the stronger vertical wind shears of linear systems imply a well organization of convection systems (Parker and Johnson [18]). The greater enrollment of mid-level dry air induces a high energy of downdraft (DCAPE). These environmental parameters of nonlinear systems are in the middle range compared with the other two morphologies.

The above results demonstrate that each morphology not only produces different SCW events, but also corresponds to different environmental conditions before convection is initiated. Overall, cellular systems tend to occur in the environment with favorable thermal condition, substantial unstable energy and low PWAT, whereas the environmental conditions favoring the initiation of linear systems feature strong vertical wind shear, high PWAT, and intense SBCIN. The environmental parameters favoring the initiation of nonlinear systems are between those of the other two morphologies. In addition, large DCAPE values of cellular and linear systems indicate a high probability of severe convective winds produced by downdraft. Therefore, further exploration of morphologies is important for understanding the three-dimensional structure, their associated SCWs and the mechanisms involved in the initiation and maintenance of convection systems.

Table 3. Comparison of environmental parameters of three storm morphologies.

Type	SBCAPE ($J\ kg^{-1}$)	MUCAPE ($J\ kg^{-1}$)	DCAPE ($J\ kg^{-1}$)	MUCIN ($J\ kg^{-1}$)	SBCIN ($J\ kg^{-1}$)	LI (K)	VWS_3km ($m\ s^{-1}$)	VWS_6km ($m\ s^{-1}$)	PWAT (mm)
Linear	**1768.0**	1684.5	590.8	49.7	56.2	−3.2	14.9	22.3	4.1
Cellular	***2558.4***	***2522.4***	***688.6***	25.4	32.7	−4.4	11.5	18.2	**3.4**
Nonlinear	1974.9	1867.8	554.3	40.5	47.4	−3.6	13.6	20.9	4.1

Table 4 presents a comparison of environmental conditions before convection initiation over different areas. The morphologies of linear systems over central east China and the United States are the same as those in previous studies (Zheng et al. [7]; Bluestein and Jain [22]). The SBCAPE (1768 J kg^{-1}) of linear systems over south China is smaller than that over central east China in Zheng et al. [7], but is larger than the SBCAPE of squall lines (1568 J kg^{-1}) over east China in Meng et al. [19] and that of the convective systems over central United States (Parker [28]). Additionally, the SBCIN (56.2 J kg^{-1}) is clearly higher than that over central east China (34 J kg^{-1}, Zheng et al. [7]) and Oklahoma (33 J kg^{-1}, Parker [28]), implying that the initiation of convection needs substantial accumulated unstable energy. LI over south China is similar to that of the squall lines over east China in Meng et al. [19], but it is lower than that over central east China in Zheng et al. [7] with more unstable

Table 4. Comparison of system environmental parameters from different studies.

Regions	Environmental parameters		SBCAPE ($J\ kg^{-1}$)	SBCIN ($J\ kg^{-1}$)	LI (K)	PWAT (cm)
South China	This study	Lines	1768	56.2	−3.2	4.1
		Cells	2558	32.7	−4.4	3.4
		No-Lines	1974	47.4	−3.6	4.1
YHRV	Zheng et al. [7]	All events	2188	23	−5.0	5.2
		Lines	1820	34	−4.3	5.4
East China	Meng et al. [19]	Squall lines	1568	61	−4.0	5.9
Oklahoma	Bluestein and Jain [22]	Lines	2260	33	−	2.8
Central plains of Unites States	Parker and Johnson [18]	LS	1009	−	−3.5	3.3
		PS	813	−	−2.2	2.4
		TS	1605	−	−5.4	3.4

environmental conditions. Among the moisture conditions, the PWAT of linear systems over south China is smaller than that over central east China and east China but is larger than that over Oklahoma and central United States.

6 CONCLUSIONS AND DISCUSSION

Composite radar reflectivity data during April to September from 2011 to 2015 have been used to investigate and classify storms and their environmental conditions in south China (18−27° N, 105−120° E). The derived storms have been divided into three main types, including linear, cellular and nonlinear systems. According to the relative locations of linear convection and stratiform region, the linear systems have been subdivided into six morphologies, including TS, BE, LS, EL, NS and PS. And then, the SCW events corresponding to each morphology have been categorized. Finally, the thermal, dynamic and water vapor environmental parameters of the three main types have been compared.

The proportion of NLs of all the total radar echoes is 46.03%. Cellular systems account for 29.45%, which is higher than that of linear systems (24.51%). Among the linear systems, the frequencies of TSs and NSs are high, whereas there are only small samples of the LSs and PSs. The monthly variation of storms show that a high frequency of convection appears in May, followed by June. The sample numbers in April and September are both small. From the geographic distribution, it is found that the maximum frequency occurs over the central and northern regions of Guangdong (the windward slopes of mountainous areas), coastal regions, the boundary regions between Guangdong and Guangxi, and the southern regions of Guangxi (with a trumpet-shaped topography), indicating the significant effect of topography on convective systems.

The main SCW events differ among the various storm morphologies. Severe convective winds account for the highest percentage (35%) of the SCW events induced by the ICs and CCs. SDHR and severe convective winds are the most common weather events associated with the TSs and BEs: the percentage of rain being higher than 45% and that of severe convective winds more than 25%. For the NSs, hail can occur simultaneously with SDHR and severe convective winds. SDHR is the most common weather event associated with the NLs, and the percentage of severe convective winds is relatively small. Comparisons of environmental physical parameters show that cellular convection systems tend to occur in the environment with favorable thermal condition, substantial unstable energy and low PWAT water vapor. However, the environmental conditions favoring the initiation of linear systems feature strong vertical wind shear, high PWAT, and intense SBCIN. The environmental parameters favoring the initiation of nonlinear systems are between those of the other two types of morphologies.

Based on the different features of morphologies, their associated SCW events and environmental conditions of storms over south China and their three-dimensional structural characteristics and evolutionary pathways will be analyzed and explored in the future study. Additionally, the synoptic patterns in low - and mid-troposphere and surface mesoscale system related to the storms are also to be analyzed to understand their formation and development mechanism.

***Acknowledgements*:** The composite radar reflectivity data, severe weather reports, precipitation observations, and surface routine observations used in the present study were provided by the National Meteorological Center, China Meteorological Administration.

REFERENCES

[1] MADDOX R A. Mesoscale convective complexes [J]. Bulletin of the American Meteorological Society, 1980, 61, 1374-1387, https://www.jstor.org/stable/26221473

[2] TAO S Y. Heavy Rainfalls in China [M]. Beijing: Science Press, 1980: 225 (in Chinese).

[3] HOUZE Jr R A. Mesoscale convective systems [J]. Reviews of Geophysics, 2004, 42(4): RG4003, https://doi.org/10.1029/2004RG000150

[4] ZHANG C X, ZHANG Q H, WANG Y Q. Climatology of hail in China: 1961-2005 [J]. Journal of Applied Meteorology and Climatology, 2008, 47(3): 795-804, https://doi.org/10.1175/2007JAMC1603.1

[5] XIE B G, ZHANG Q H, WANG Y Q. Observed characteristics of hail size in four regions in China during 1980-2005 [J]. Journal of Climate, 2010, 23(18): 4973-4982, https://doi.org/10.1175/2010JCLI3600.1

[6] YU R, ZHANG X L, LI G P, et al. Analysis of frequency variation of thunderstorm, hail and gale wind in eastern China from 1971 to 2000 [J]. Meteorological Monthly (in Chinese), 2011, 38(10): 1207-1216, https://doi.org/10.7519/j.issn.1000-0526.2012.10.006

[7] ZHENG L L, SUN J H, ZHANG X L, et al. Organizational modes of mesoscale convective systems over central east China [J]. Weather and Forecasting, 2013, 28(5): 1081-1098, https://doi.org/10.1175/WAF-D-12-00088.1

[8] TOLLERUD E I, COLLANDER R S. Mesoscale convective systems and extreme rainfall in the central United States [C]// Extreme Hydroloeical Events: Precipitation, Floods and Droughts. Yokohama: International Association of Hydrological Sciences, 1993, 213: 11-19.

[9] DOSWELL C A. Synoptic-scale environments associated with high plains severe thunderstorms [J]. Bulletin of the American Meteorological Society, 1980, 61(11): 1388-1400.

[10] SCHUMACHER R S, JOHNSON R H. Organization and environmental properties of extreme-rain-producing mesoscale convective systems [J]. Monthly Weather Review, 2005, 133(4): 961-976, https://doi.org/10.1175/MWR2899.1

[11] SHIBAGAKI Y, YABANAKA M D, SHIMIZU S, et al. Meso-β to meso-γ-scale wind circulations associated with

precipitating clouds near baiu front observed by the MU and meteorological radars [J]. Journal of the Meteorological Society of Japan, 2000, 78(1): 69-91, https://doi.org/10.2151/jmsj1965.78.1_69

[12] AUGUSTINE J A, HOWARD K W. Mesoscale convective complexes over the United States during 1985 [J]. Monthly Weather Review, 1988, 116(3): 685-701, https://doi. org/ 10.1175 / 1520-0493(1988)116%3c0685: MCCOTU%3e2.0.CO;2

[13] LAING A G, FRITSCH J M. The global population of mesoscale convective complexes [J]. Quarterly Journal of the Royal Meteorological Society, 1997, 123(538): 389-405. https://doi.org/10.1002/qj.49712353807

[14] ANDERSON C J, ARRITT R W. Mesoscale convective complexes and persistent elongated convective systems over the United States during 1992 and 1993 [J]. Monthly Weather Review, 1998, 126(3): 578-599. https://doi. org / 10.1175/1520-0493(1998)126<0578:MCCAPE>2.0.CO;2

[15] JIRAK I L, COTTON W R, MCANELLY R L. Satellite and radar survey of mesoscale convective system development [J]. Monthly Weather Review, 2003, 131 (10): 2428-2449, https://doi.org/10.1175/1520-0493(2003) 131%3C2428:SARSOM%3E2.0.CO;2

[16] GOYENS C, LAUWAET D, SCHRÖDER M, et al. Tracking mesoscale convective systems in the Sahel: Relation between cloud parameters and precipitation [J]. International Journal of Climatology, 2012, 32(12): 1921-1934, https://doi.org/10.1002/joc.2407

[17] ZHUO H, ZHAO P, LI C H, et al. Analysis of climatic characteristics of mesoscale convective system over the lower reaches of the Yellow River during summer [J]. Chinese Journal of Atmospheric Sciences (in Chinese), 2012, 36(6): 1112-1122, https://doi. org / 10.3878 / j. issn.1006-9895.2011.11174

[18] PARKER M D, JOHNSON R H. Organizational modes of midlatitude mesoscale convective systems [J]. Monthly Weather Review, 2000, 128(10): 3413-3436, https://doi. org/10.1175/1520-0493(2001)129<3413:OMOMMC>2.0. CO;2

[19] MENG Z Y, YAN D C, ZHANG Y J. General features of squall lines in east China [J]. Monthly Weather Review, 2013, 141(5): 1629-1647, https://doi.org/10.1175/MWR-D-12-00208.1

[20] LI S, MENG Z Y, WU N G. A preliminary study on the organizational modes of mesoscale convective systems associated with warm-sector heavy rainfall in South China [J]. Journal of Geophysical Research: Atmospheres, 2021, 126(16): e2021JD034587, https://doi. org/10.1029/2021JD034587

[21] CHEN Y R X, LUO Y L, LIU B. General features and synoptic-scale environments of mesoscale convective systems over South China during the 2013-2017 pre-summer rainy seasons [J]. Atmospheric Research, 2022, 266: 105954, https://doi. org / 10.1016 / j. atmosres.2021.105954

[22] BLUESTEIN H B, JAIN M H. Formation of mesoscale lines of precipitation: Severe squall lines in Oklahoma during the spring [J]. Journal of the Atmospheric Sciences, 1985, 42(16): 1711-1732, https://doi. org / 10.1175/1520-0469(1985)042<1711:FOMLOP>2.0.CO;2

[23] BLANCHARD D O. Mesoscale convective patterns of the southern high plains [J]. Bulletin of the American Meteorological Society, 1990, 71(7): 994-1005, https://doi. org / 10.1175 / 1520-0477(1990)071<0994: MCPOTS> 2.0.CO;2

[24] LOEHRER S M, JOHNSON R H. Surface pressure and precipitation life cycle characteristics of pre-storm mesoscale convective systems [J]. Monthly Weather Review, 1995, 123(3): 600-621, https://doi. org / 10.1175 / 1520-0493(1995)123%3C0600:SPAPLC%3E2.0.CO;2

[25] WANG H, LUO Y L, JOU B J D. Initiation, maintenance, and properties of convection in an extreme rainfall event during SCMREX: Observational analysis [J]. Journal of Geophysical Research: Atmospheres, 2014, 119(23): 13206-13232, https://doi.org/10.1002/2014JD022339

[26] YANG X L, SUN J H. Organizational modes of severe wind-producing convective systems over North China [J]. Advances in Atmospheric Sciences, 2018, 35(5): 540-549, https://doi.org/10.1007/s00376-017-7114-2

[27] GALLUS Jr W A, SNOOK N A, JOHNSON E V. Spring and summer severe weather reports over the midwest as a function of convective mode: A preliminary study [J]. Weather and Forecasting, 2008, 23(1): 101-113, https://doi.org/10.1175/2007WAF2006120.1

[28] PARKER M D. Simulated convective lines with parallel stratiform precipitation, Part I: An archetype for convection in along-line shear [J]. Journal of the Atmospheric Sciences, 2007, 64(2): 267-288, https://doi. org/10.1175/JAS3853.1

[29] DUDA J D, GALLUS Jr W A. Spring and summer Midwestern severe weather reports in supercells compared to other morphologies [J]. Weather and Forecasting, 2010, 25(1): 190-206, https://doi. org / 10.1175/2009WAF2222338.1

[30] LOMBARDO K A, COLLE B A. Convective storm structures and ambient conditions associated with severe weather over the northeast United States [J]. Weather and Forecasting, 2011, 26(6): 940-956, https://doi. org / 10.1175/WAF-D-11-00002.1

[31] FUJITA T T. Manual of downburst identification for project NIMROD [R]. Chicago: University of Chicago, 1978.

[32] TRAPP R J, TESSENDORF S A, GODFREY E S, et al. Tornadoes from squall lines and bow echoes, Part I: Climatological distribution [J]. Weather and Forecasting, 2005, 20(1), 23-34, https://doi.org/10.1175/WAF-835.1

[33] MOLLER A R, DOSWELL III C A, FOSTER M P, et al. The operational recognition of supercell thunderstorm environments and storm structures [J]. Weather and Forecasting, 1994, 9(3): 327-347, https://doi.org/10.1175/1520-0434(1994)009<0327:TOROST>2.0.CO;2

[34] PETTET C R, JOHNSON R H. Airflow and precipitation structure of two leading stratiform mesoscale convective systems determined from operational datasets [J]. Weather and Forecasting, 2003, 18(5): 685-699, https://doi. org / 10.1175 / 1520-0434(2003)018<0685: AAPSOT> 2.0.CO;2

[35] MENG Z Y, ZHANG Y J. On the squall lines preceding landfalling tropical cyclones in China [J]. Monthly Weather Review, 2012, 140(2): 445-470, https://doi. org / 10.1175/MWR-D-10-05080.1

[36] TAO S Y, DING Y H. Observational evidence of the influence of the Qinghai-Xizang (Tibet) Plateau on the occurrence of heavy rain and severe convective storms in

China [J]. Bulletin of the American Meteorological Society, 1981, 62(1): 23-30, https://doi.org/10.1175/1520-0477(1981)062<0023:OEOTIO>2.0.CO;2

[37] NINOMIYA K, AKIYAMA T. Multi-scale features of Baiu, the summer monsoon over Japan and the East Asia [J]. Journal of the Meteorological Society of Japan, 1992, 70(1B): 467-495, https://doi.org/10.2151/jmsj1965.70.1B_467

[38] GEERTS B. Mesoscale convective systems in the southeast United States during 1994-95: A survey [J]. Weather and Forecasting, 1998, 13(3): 860-869, https://doi. org / 10.1175 / 1520-0434(1998)013<0860: MCSITS>2.0.CO;2

[39] YANG R Y, ZHANG Y C, SUN J H, et al. The comparison of statistical features and synoptic circulations between the eastward-propagating and quasi-stationary MCSs during the warm season around the second-step terrain along the middle reaches of the Yangtze River [J]. Science China Earth Sciences, 2020, 63 (8): 1209-1222, https://doi.org/10.1007/s11430-018-9385-3

[40] LEE J W. Tornado proximity soundings from the NCEP/NCAR reanalysis data [D]. Norman: University of Oklahoma, 2002: 60-61.

[41] BROOKS H E, LEE J W, CRAVEN J P. The spatial distribution of severe thunderstorm and tornado environments from global reanalysis data [J]. Atmospheric Research, 2003, 67-68: 73-94, https://doi.org/10.1016/S0169-8095(03)00045-0

[42] JOHNSON R H, BRESCH J F. Diagnosed characteristics of precipitation systems over Taiwan, China during the May - June 1987 TAMEX [J]. Monthly Weather Review, 1991, 119(11): 2540-2557, https://doi.org/10.1175/1520-0493(1991)119<2540:DCOPSO>2.0.CO;2

[43] PAN Y J, ZHAO K, PAN Y N. Single-Doppler radar observation of a heavy precipitation supercell on a severe squall line [J]. Acta Meteorologica Sinica (in Chinese), 2008, 66(4): 621-636, http://dx. doi. org / 10.11676 / qxxb2008.059

[44] LUO Y L. Advances in understanding the early-summer heavy rainfall over South China [M]// Chang C P, KUO H C, LAU N C, et al (eds), The Global Monsoon System: Research and Forecast. Singapore: World Scientific, 2017: 215-226.

[45] WU M W, LUO Y L. Mesoscale observational analysis of lifting mechanism of a warm-sector convective system producing the maximal daily precipitation in China mainland during pre-summer rainy season of 2015 [J]. Journal of Meteorological Research, 2016, 30(5): 719-736, https://doi.org/10.1007/s13351-016-6089-8

[46] BAI L Q, CHEN G X, HUANG L. Convection initiation in monsoon coastal areas (South China) [J]. Geophysical Research Letters, 2020, 47(11): e2020GL087035, https://doi.org/10.1029/2020GL087035

[47] CHEN G X, SHA W M, IWASAKI T, et al. Diurnal cycle of a heavy rainfall corridor over East Asia [J]. Monthly Weather Review, 2017, 145(8): 3365-3389, https://doi.org/10.1175/MWR-D-16-0423.1

[48] DU Y, CHEN G X. Climatology of low-level jets and their impact on rainfall over southern China during the early-summer rainy season [J]. Journal of Climate, 2019, 32(24): 8813-8833, https://doi. org / 10.1175 / JCLI-D-19-0306.1

[49] DU Y, CHEN G X, HAN B, et al. Convection initiation and growth at the coast of South China, Part II: Effects of the terrain, coastline, and cold pools [J]. Monthly Weather Review, 2020, 148(9): 3871-3892, https://doi.org/10.1175/MWR-D-20-0090.1

[50] YANG X L, SUN J H, ZHENG Y G. A 5-yr climatology of severe convective wind events over China [J]. Weather and Forecasting, 2017, 32(4): 1289-1299, https://doi. org/10.1175/WAF-D-16-0101.1

[51] LI X F, ZHANG Q H, ZOU T, et al. Climatology of hail frequency and size in China, 1980-2015 [J]. Journal of Applied Meteorology and Climatology, 2018, 57(4): 875-887, https://doi.org/10.1175/JAMC-D-17-0208.1

[52] CHEN J, ZHENG Y G, ZHANG X L, et al. Analysis of the climatological distribution and diurnal variations of the short-duration heavy rain and its relation with diurnal variation of the MCSs over China during the warm season [J]. Acta Meteorologica Sinica (in Chinese), 2013, 71(3): 367-382, https://doi.org/10.11676/qxxb2013.035

Citation: ZHANG Yuan-chun, LU Rong, SUN Jian-hua, et al. Organizational Modes and Environmental Conditions of the Severe Convective Weathers Produced by the Mesoscale Convective Systems in South China [J]. Journal of Tropical Meteorology, 2023, 29 (1): 26-38, https://doi.org/10.46267/j.1006-8775.2023.003